

The Padre Miguel Ignimbrite Suite, central Honduras: Paleomagnetism, geochronology, and tectonic implications

Roberto S. Molina Garza ^{a,*}, Douwe J.J. van Hinsbergen ^b, Robert D. Rogers ^c, Morgan Ganerød ^d, Mark J. Dekkers ^e

^a Centro de Geociencias, Universidad Nacional Autónoma de México, Blvd. Juriquilla 3001, Querétaro, Mexico

^b Physics of Geological Processes, University of Oslo, Sem Saelands vei 24, 0316 Oslo, Norway

^c Department of Geology, California State University, Stanislaus, 801 W. Monte Vista Ave. Turlock, CA, USA

^d Geological Survey of Norway NGU, Leiv Eirikssons Vei 39, 7491 Trondheim, Norway

^e Paleomagnetic Laboratory Fort Hoofddijk, Utrecht University, Budapestlaan 17, 3584 CD Utrecht, Netherlands

ARTICLE INFO

Article history:

Received 2 February 2012

Received in revised form 3 July 2012

Accepted 8 August 2012

Available online 21 August 2012

Keywords:

Honduras

Paleomagnetism

Caribbean

Strike-slip deformation

⁴⁰Ar/³⁹Ar geochronology

ABSTRACT

The Padre Miguel Group in western Honduras is a silicic volcanic sequence that forms part of the Central American Miocene volcanic arc built on the Chortis continental fragment. We report new ⁴⁰Ar/³⁹Ar data of 16.1 ± 0.2 Ma and 14.42 ± 0.08 Ma for the Padre Miguel Group, and present paleomagnetic data for 36 cooling units (mainly ignimbrites) from localities north and northeast of the capital city of Tegucigalpa. These rocks are characterized by univectorial characteristic magnetization carried mainly by low-Ti titanomagnetites, or two component magnetizations with a minor secondary overprint. Dual polarity magnetizations suggest that it is a primary thermo-remnant and the obtained data scatter can be straightforwardly explained by paleosecular variation. The overall mean of 33 selected sites (14.39°N , 87.14°W) defines a paleomagnetic pole at $\text{lat} = 80.0^\circ\text{N}$, $\text{lon} = 142.9^\circ\text{E}$ ($K = 24.5$, $A_{95} = 5.2^\circ$). The overall mean compared with the North America expected direction indicates statistically insignificant rotation and inclination anomaly ($R = -4.1^\circ \pm 6.1^\circ$ and an $F = -8.6^\circ \pm 11.3^\circ$). Restoring 255 km of sinistral slip in the Polochic–Motagua fault system, as suggested by Cayman Trough reconstructions since 15 Ma, brings the mid-Miocene arcs of southern Mexico (Oaxaca) and the Central America ignimbrite province into alignment; this is consistent with a derivation of the Chortis Block from southern Mexico. Our paleomagnetic and geochronological studies hence support models that explain the offset of the Miocene ignimbrite belt of Central America by post-Middle Miocene displacement of the Chortis Block relative to North America.

© 2012 Elsevier B.V. All rights reserved.

1. Introduction

It has been recognized for some time that regional inter-plate domains, such as the Caribbean and the Mediterranean, are regions of the world where rigid-body plate motions fail to describe much of the tectonic processes. In these settings, paleomagnetism is a useful tool for determining intra-plate deformation and regional block rotations. The Chortis Block, which includes southern Guatemala, Honduras, El Salvador, northern Nicaragua, and the Nicaragua rise, is a large fragment of continental crust in the western Caribbean plate (Fig. 1; Case and Holcombe, 1980; Dengo, 1969). A Pacific origin for the Caribbean plate is well documented (Pindell and Kennan, 2009; Pindell et al., 1988; Wadge and Burke, 1983), but the Chortis Block did not become part of the Caribbean plate until sometime in the Paleogene (Pindell et al., 1988, 2011).

It is generally accepted that oblique plate convergence and subduction of the Kula–Farallon and Farallon–Pacific spreading centers resulted in complex plate interactions in the western margin of North America in

the Cenozoic (e.g., Engebreston et al., 1985; Mammerickx and Klitgord, 1982). In turn, changes in plate boundary forces caused fragmentation of continental crust and truncation of the southwest margin of North America. Various authors have thus proposed that Farallon plate convergence, evolution of the Caribbean, and deformation in the southwest Mexico margin are closely linked processes (e.g., Herrmann et al., 1994; Meschede and Frisch, 1998; Pindell and Barrett, 1990; Wadge and Burke, 1983).

Several authors support the hypothesis that the Chortis Block was originally part of the southern Mexico continental assemblage, and its present position in the Caribbean plate resulted from the fragmentation and plate reorganization process in the western margin of the continent described above (Karig-Cordwell et al., 1978; Malfait and Dinkelman, 1972; Schaaf et al., 1995). The plate boundary of the Caribbean and North American plates is formed by a left-lateral transform boundary that contains the Cayman pull-apart basin and the Swan Island transform. This transform boundary between the Chortis Block and the Maya Block of the North American plate includes the Polochic–Motagua fault system, which is linked to the Swan Island fault zone (DeMets et al., 2007; Guzmán-Speziale and Meneses-Rocha, 2000; Rogers and Mann, 2007; Fig. 1, inset). An earlier westward

* Corresponding author.

E-mail address: rmolina@geociencias.unam.mx (R.S.M. Garza).

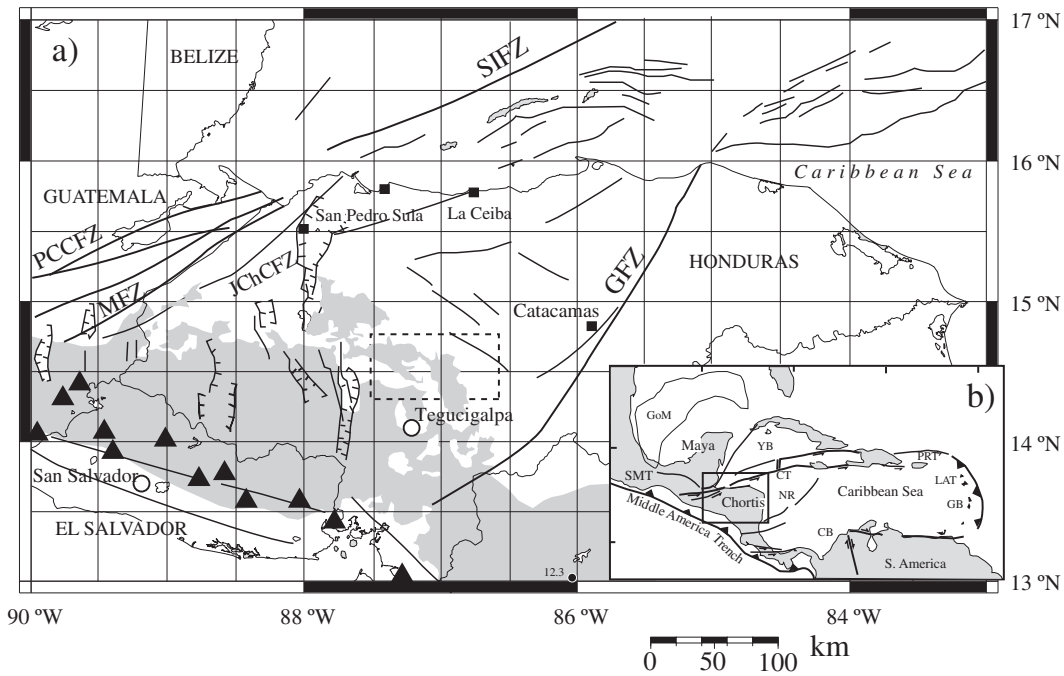


Fig. 1. a) Simplified tectonic map of the Chortis Block showing distribution of the Central America Cenozoic ignimbrite province (gray). Triangles indicate the modern volcanic arc. PCCFZ = Polochic–Cuilco–Chixoy fault zone; JChCFZ = Jocotán–Chamalecón–La Ceiba fault zone; SIFZ = Swan Island fault zone; MFZ = Motagua fault zone; GFZ = Guayape fault zone. The box marks the study area. b) Inset: schematic map of the Caribbean plate showing location of the Chortis Block. SMT = Southern Mexico Terranes; NR = Nicaragua Rise; YB = Yucatán Basin; GB = Guayana basin; LAT = Lesser Antilles trench; CB = Colombian basin; GoM = Gulf of México.

continuation of the Polochic–Motagua fault zone that accommodated motion of Chortis away from southern Mexico probably became reactivated as subduction zone, now occupied by the Middle America Trench (e.g. Pindell and Barrett, 1990; Pindell et al., 2011; Wadge and Burke, 1983). The transfer of the Chortis Block from the North American plate to the Caribbean plate probably occurred in the Paleogene, and resulted in internal deformation of the crustal blocks involved (Pindell and Barrett, 1990; Wadge and Burke, 1983). Alternative models (e.g. Keppie and Moran-Zenteno, 2005) suggest that the Chortis Continental Block is not genetically linked to southern Mexico, but was in an ill-defined, intra-Pacific position instead until the Paleogene. Nevertheless, Silva-Romo and Mendoza-Rosales (2009) discuss the evidence for alternative models, concluding that detachment of Chortis from southern Mexico is the most viable.

Recently, Rogers et al. (2007) demonstrated that the Chortis Block is composed of a nuclear Central Chortis terrane with Precambrian–Paleozoic basement, an Eastern Chortis terrane characterized by Jurassic metasedimentary rocks, and the Siuna terrane composed of oceanic island arc rocks in the east. Rogers et al. (2007) also recognize a Northern Chortis terrane, which is characterized by magmatic overprint of the Eastern and Central Chortis terrane assemblages, and the Southern Chortis terrane characterized by oceanic island arc rocks. This collage was apparently assembled by Late Cretaceous time. Chortis shares with southern Mexico similar Grenvillian and Paleozoic poly-metamorphic basements (Manton, 1996; Ratschbacher et al., 2009), Jurassic–Cretaceous stratigraphy, and alignment of magnetic and structural features (Rogers et al., 2007). Nonetheless, the reconstruction of Chortis to its pre Cenozoic position is not straightforward, and several models have been proposed (e.g., Rogers et al., 2007; Silva-Romo, 2008; Fig. 2). Previous authors have noted that refining the models requires additional paleomagnetic and isotopic age data from Chortis. Ortega-Gutiérrez et al. (2007) recognize fault-bounded geologic entities in the region generally referred to as Chortis and its northern boundary with the Maya Block. These authors recognize that the tectonic domain between Chortis proper and the Maya Block is a series of crustal slices composed of metamorphic basement assemblages

located between the Polochic–Cuilco–Chixoy fault system in the north, and the Jocotán–Chamalecón–La Ceiba faults in the south (Fig. 1).

In this paper we present new $^{40}\text{Ar}/^{39}\text{Ar}$ geochronological and paleomagnetic data for the Miocene Padre Miguel Group of central Honduras, and discuss the implications of these data for the Neogene evolution of the Chortis Block and its relationship with southern Mexico.

2. Geological setting

The Padre Miguel Group is part of the Central America Ignimbrite Province, which extends from Guatemala to Nicaragua east of and nearly parallel to the modern Central America arc (Fig. 1). This unit was first defined in southeastern Guatemala (Burkart and Clemons, 1973; Williams et al., 1964), and blankets a large area of the Central America highlands (Williams and McBirney, 1969). Jordan et al. (2007) report two major magmatic pulses in this province, one of Eocene age and a larger one of Middle Miocene age. The silicic ignimbrites show clear subduction geochemistry, with ample evidence of continental crust influence. Rogers et al. (2002) suggest that voluminous ignimbrite emplacement is related to an episode of fast convergence at the Middle America trench between 10 and 18 Ma. Heiken et al. (1991) reported two K–Ar ages of ca. 14 Ma for biotite separates from two welded ignimbrites near the base of this unit in northwestern Honduras. Elming et al. (2001) report K–Ar and $^{40}\text{Ar}/^{39}\text{Ar}$ ages for Miocene volcanic rocks in Nicaragua, assigned to El Coyal Group of ~18 Ma. Published and unpublished K–Ar ages for the Padre Miguel Group (PMG) in Honduras and Nicaragua were compiled by Rogers (2003). They range from 10.4 to 18.9 Ma, with a clear concentration of ages at about 14 and 18 Ma (Ehrenborg, 1986; Emmet, 1983).

The Padre Miguel Group covers an area of approximately 70,000 km² in Honduras, and is well exposed in the Honduras highlands between Tegucigalpa and Talanga (Fig. 3). The Padre Miguel Group in the field area consists mostly of rhyolitic pyroclastic flow deposits and minor epiclastic rocks and lavas, covered by younger basaltic and andesitic rocks. The sequence has an estimated maximum thickness of ~2000 m

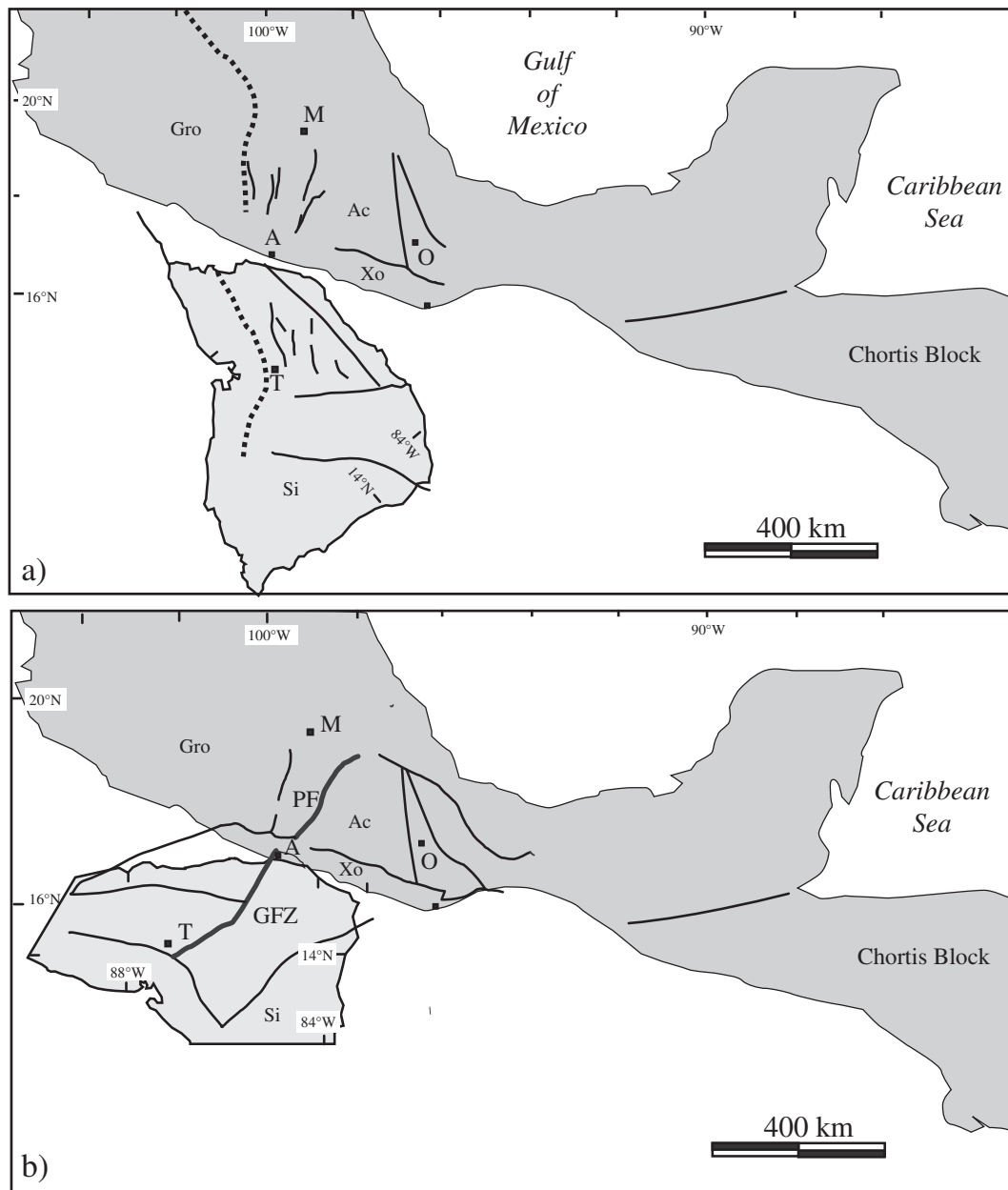


Fig. 2. Alternative reconstructions of the Chortis Block relative to southern Mexico terranes, after a) Rogers et al. (2007) and b) Silva-Romo (2008). Rogers et al. (2007) notice the alignment of the magnetic features (dotted line), while Silva-Romo (2008) aligns the Guayape (GFZ) and Papalutla faults (PF). Other symbols are: M = Mexico City; A = Acapulco; O = Oaxaca; T = Tegucigalpa; Ac = Acatlán Complex; Xo = Xolapa terrane; Gro = Guerrero terrane; Si = Siuna terrane.

(Heiken et al., 1991; Williams and McBirney, 1969). It overlies Cretaceous clastic and carbonate strata or Paleozoic (?) metamorphic rocks with a pronounced angular unconformity. The ignimbrite succession is affected by a system of inactive nearly N–S trending faults, causing variable, but gentle tilt of the sequence (Rogers and Mann, 2007). Extension has been explained as the result of distributed strain caused by relative motion of the Caribbean plate with respect to Chortis, which remained pinned to the Cocos and North America plates (Plafker, 1976); a model of rotation of the trailing edge of the Caribbean plate (Chortis Block) around the Polochic–Motagua fault system has also been proposed (Burkart and Self, 1985). In central Honduras, Rogers et al. (2002) recognize an active western horst and graben province, a central tectonically stable province, and a mountainous heavily dissected eastern province. This is supported by GPS (Rodríguez et al., 2009) and geomorphologic observations (Rogers et al., 2002).

3. Sampling

Samples for this study were collected from the Honduras highlands mostly along the main road from Tegucigalpa to Catacamas, north and northeast of Tegucigalpa (Fig. 3), in what is considered the central tectonically stable region of the Chortis Block (Rogers et al., 2002). Sites 1 through 8 were sampled using a portable water-cooled drill, and samples were oriented in-situ with an orientation device. Hand samples were collected in the remaining 33 sites, oriented with a Brunton compass. The study includes a total of 188 samples in 41 sites, in three main areas around the small city of Talanga. Each site corresponds to a road cut, or a fresh natural outcrop, in a single cooling unit over an area of 10 to 20 m². Care was taken in the field to ensure each site is a different unit. Block-sample sites consist of 3 to 5 samples, drilled sites contain 6

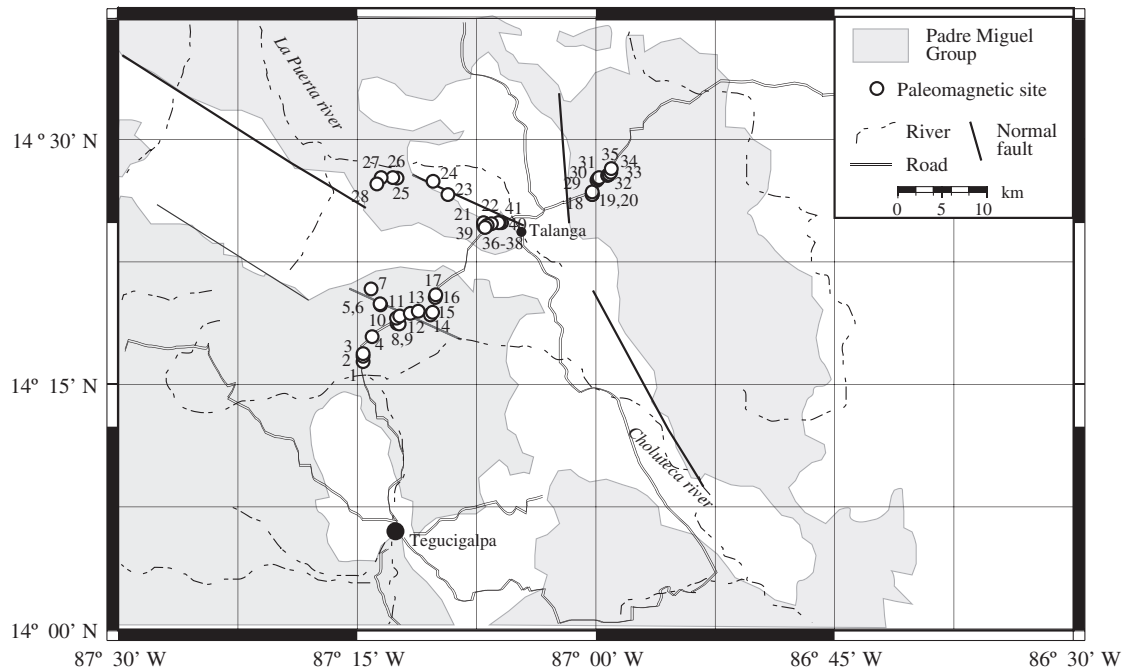


Fig. 3. Simplified map of central Honduras showing distribution of the Padre Miguel Group (gray shading) and paleomagnetic sampling sites.

to 8 samples. Where possible, sun compass orientations were determined and geographic azimuths calculated; no systematic differences in orientations were observed. Standard paleomagnetic specimens (cylinders 2.5 cm in diameter and 2.1 cm tall) were prepared in the laboratory from each sample. Sites 1–17 are integrated in a western area, sites 21–28 and 36–41 in a central area, and sites 18–20 and 29–35 in an eastern area (Fig. 3). Samples from paleomagnetic sites TT17 and TT31 were used for $^{40}\text{Ar}/^{39}\text{Ar}$ geochronology.

4. $^{40}\text{Ar}/^{39}\text{Ar}$ geochronology

4.1. Analytical protocol

The samples were crushed and sieved to isolate grains of 180–250 μm . The mineral separates were washed in acetone several times and rinsed with distilled water, and finally fresh inclusion-free feldspar grains were handpicked under the binocular microscope. The samples were packed in aluminum capsules together with the Taylor Creek rhyolite (TC) flux monitor standard (between each 5th sample, every ~8 mm) and zero aged K_2SO_4 and CaF_2 , and the transformation $^{39}\text{K}(n, p) ^{39}\text{Ar}$ was performed during irradiation at the IFE nuclear facility located in Kjeller, Norway. The correction factors for the production of isotopes from Ca were determined to be $(^{39}\text{Ar}/^{37}\text{Ar})\text{Ca} = (6.2523 \pm 0.4856) \times 10^{-4}$, $(^{36}\text{Ar}/^{37}\text{Ar})\text{Ca} = (5.9112 \pm 1.7343) \times 10^{-4}$ and $(^{40}\text{Ar}/^{39}\text{Ar})\text{K} = (1.7005302 \pm 0.3251701) \times 10^{-1}$ for the production of K. The samples were step heated in the $^{40}\text{Ar}/^{39}\text{Ar}$ lab at the Geological Survey of Norway using a double-vacuumed resistance furnace (Heine type). The extracted gases were gathered (SAES GP-10 pumps) for the first 2 min, then for 9 min in a separate part of the extraction line (SAES GP-10 pumps). The gas was analyzed with an MAP 215–50 mass spectrometer. The peaks were determined during peak hopping (at least 8 cycles) on the different masses ($^{41}\text{--}^{35}\text{Ar}$) on a Balzers electron multiplier. The blanks were measured at temperatures 450, 700, 1000, 1130 and 1280 $^\circ\text{C}$, the blanks and associated errors for the respective temperature steps for the unknowns were determined using linear interpolation. Subtraction for blanks, correction for mass fractionation, ^{37}Ar and ^{39}Ar decay, and neutron-induced interference reactions produced in the reactor were done using in-house

software (Age Monster 2010, written by M. Ganerød). It implements the equations of McDougall and Harrison (1999), and the total decay constant for ^{40}K after Renne et al. (2010). We calculated J-values relative to an age of 28.619 ± 0.034 Ma for the TC monitor (Renne et al., 2010). The mass fractionation was determined using an air pipette mounted within the extraction line, and the mass discrimination value is based on the $^{40}\text{Ar}/^{36}\text{Ar}$ ratio from Lee et al. (2006) using a power law function. We calculated weighted mean plateau ages (WMPA), weighting on the inverse of the variance at locations where consecutive steps were within the $\text{abs}(\text{age}_n - \text{age}_{n+1}) < 1.96 * ((\sigma_n)^2 + (\sigma_{n+1})^2)^{0.5}$ error envelope. Uncertainties from inlet intensities, blanks, mass discrimination value, salts, trapped constants and every mass balance calculation are propagated into the final age uncertainty.

4.2. Results

K-feldspar separates from the two ignimbrites, samples 061609B and 061709B, were analyzed by the furnace step-heating method, and correspond to paleomagnetic sampling sites TT17 (crystal rich ignimbrite) and TT31, respectively. The spectrum, K/Ca ratio (calculated from $^{39}\text{Ar}_k/^{37}\text{Ar}_{Ca}$) and inverse isochron results are shown in Fig. 4a and b, and the main results are summarized in Table 1. The raw experimental results can be found in a supplemental data file. All ages are reported at the 1.96σ confidence level.

Sample 061609B gives concordant apparent ages for most of the released cumulative $\%^{39}\text{Ar}$ and yields a weighed mean plateau age of 14.42 ± 0.08 Ma. The inverse isochron result gives an intercept through the modern atmospheric value, and the age is within error of the plateau age. Nonetheless, the confidence interval for this result is entirely within an interval of normal polarity in the geomagnetic polarity time scale (Cande and Kent, 1995), and the characteristic magnetization of the unit samples is of reverse polarity. This suggests a more likely age of ~14.6 Ma, within chron C5ADr. The release spectrum from sample 061709B shows a decline in apparent ages in the first part of the experiment, a typical pattern for excess Ar, however, overlapping apparent ages are found at higher temperature steps. From those steps we calculated a weighted mean age of $16.1 \pm$

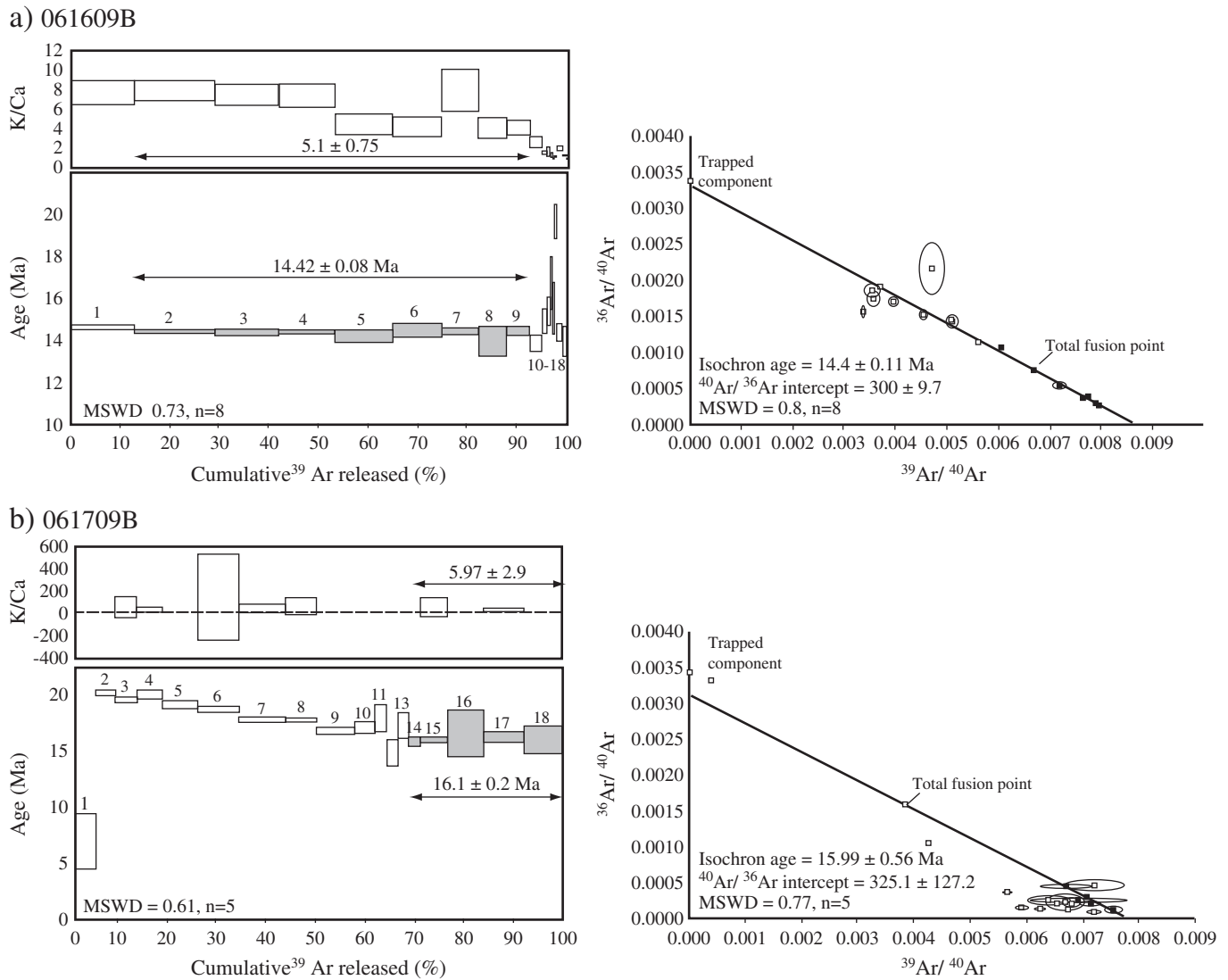


Fig. 4. $^{40}\text{Ar}/^{39}\text{Ar}$ age spectrums (below) and K/Ca ratios (above) for furnace step heating experiments from sample a) 061609B and b) 061709B. The error bars at each step and the calculated ages are shown at the 95% confidence level (1.96σ). The numbers above each bar represent the experiment number in the supplemental data file.

0.2 Ma, but consists only of 31.5% of cumulative ^{39}Ar and is not a strict plateau. The same steps yield an inverse isochron age of 15.99 ± 0.56 Ma and the intercept overlaps with modern atmospheric value. Due to a high radiogenic part of total ^{40}Ar , the $^{36}\text{Ar}/^{40}\text{Ar}$ intercept is poorly defined and has a large uncertainty, and therefore cannot exclude whether there might be excess ^{40}Ar in the aforementioned weighted mean age. However, the correspondence between the isochron age and the weighted mean age seems to militate against an excess component, and we interpret that the trapped air component in the weighted mean age is successfully corrected for and we use that in the following discussion.

5. Paleomagnetic analysis

5.1. Sampling and methods

To constrain the paleomagnetic interpretation, and to shed light on the magnetic mineralogy, several rock magnetic experiments were carried out on selected samples. These include measurement of hysteresis loops and back-field curves at room temperature, determination of acquisition curves of the isothermal remanent magnetization (IRM) also at room temperature, measurement of the temperature dependence of the low-field susceptibility, and finally measurements

Table 1
Summary of $^{40}\text{Ar}/^{39}\text{Ar}$ furnace step heating experiments. Ages are in Ma.

Sample	Steps	Spectrum analysis				Inverse isochron analysis						
		$^{39}\text{Ar}(k)$ %	Age	$\pm 2\sigma^a$	MSWD	K/Ca	$\pm 2\sigma^a$	Age	$\pm 2\sigma^a$	MSWD	Intercept	$\pm 2\sigma$
061609B	2–9	79.68	14.42	0.05/0.08/0.09	0.73	5.1	0.75	14.4	0.08/0.11/0.12	0.8	300.8	9.7
061709B	14–18	31.47	16.1	0.18/0.197/0.204	0.612	5.97	2.9	15.99	0.56/0.56/0.57	0.77	325.1	127

^a Uncertainties are reported as analytical/internal/external errors. The internal error includes the analytical error and the error on the J-value (analytical + fluence monitor uncertainty). External error also includes the uncertainty on the total 40 K decay constant. The K/Ca ratios are calculated from $^{39}\text{Ar}/^{37}\text{ArCa}$.

of magnetization versus temperature in a Curie balance. The temperature dependent measurements were carried out in air. Samples from sites TT9, TT17, TT25, TT36 and TT41 were selected for rock magnetic measurements (Table 2).

The susceptibility versus temperature data was measured with a CS2-3 high-temperature attachment to a KLY-3 susceptometer (AGICO, Brno, Czech Republic), the sensitivity of the instrument is $4e^{-8}$ SI for a nominal volume of 10 cm³, the heating and cooling rates were set to 'medium', equivalent to ~8 °C/min. To check for chemical alteration during annealing runs to 400 °C and cooling back to room temperature were followed by a run of up to 700 °C (and cooling back to room temperature). Magnetization versus temperature measurements (thermomagnetic analysis) were performed with a modified horizontal translation Curie balance that employs a sinusoidal

cycling field rather than a fixed field (Mullender et al., 1993). This ensures a very good drift correction resulting in a high sensitivity of (instrumental noise level ~5e⁻⁹Am²). Again, to check for chemical alteration during heating, the so-called segmented run protocol was adopted in which the sample is stepwise heated to increasingly elevated temperatures with intermittent cooling to 100 °C which is lower than the maximum temperature of each segment. Heating and cooling rates are 10 °C/min; maximum temperatures (°C) of subsequent heating cycles are (cooling temperatures in °C indicated between brackets): 250 (150), 380 (280), 460 (360), 540 (440), 620 (500) and 700 (room temperatures).

Hysteresis loops and back-field demagnetization curves were measured with a Princeton MicroMag Model 2900 alternating gradient magnetometer. Instrumental noise level is approximately 2e⁻⁹Am²

Table 2
Paleomagnetic data and statistical parameters.

Site	Lat. (N)	Long. (W)	Samples	In situ				Tilt corrected			
				Dec (°)	Inc (°)	k	α95	Stk,dip	Dec (°)	Inc (°)	
1	14.27	87.24	7\9\9	358.8	14.7	75.4	7.0	300, 7	359.5	8.7	
2	14.28	87.24	7\8\8	348.9	7.9	216.9	4.1	302, 9	349.4	1.3	
3	14.28	87.24	6\9\9	352.3	10.5	191.3	4.9	302, 9	353.0	3.5	
4	14.3	87.23	7\9\9	355.9	8.4	177.6	4.5	325, 06	356.5	5.3	
5	14.33	87.23	7\8\8	197.5	-2.1	185.7	4.4	54, 10	198.2	-8.0	
6	14.33	87.23	5\6\6	188.2	-15.2	63.7	9.7	54, 10	190.6	-22.2	
7	14.35	87.24	4\5\5	183.7	-0.4	129.2	8.1	54, 10	184.2	-8.1	
			9\11\11	186.1	-9.1	94.7	5.8		187.6	-16.4	
8 ^a	14.31	87.21	5\5\5	20.0	19.2	19.9	42.6	Sub hoz	20.0	19.2	
9	14.31	87.21	3\5\5	337.7	17.8	61.5	15.9	Sub hoz	337.7	17.8	
10	14.32	87.21	5\6\6	351.9	25.5	37.1	12.7	Sub hoz	351.9	25.5	
11	14.32	87.21	5\7\7	338.5	36.5	47.1	11.3	Sub hoz	338.5	36.5	
12	14.32	87.19	4\6\8	180.6	-16.3	110.1	8.8	345,8			
13	14.32	87.19	5\5\5	180.9	-15.2	85.9	8.3	345,8			
			9\11\13	180.8	-15.7	93.9	5.4		182.8	-13.4	
14	14.32	87.17	4\6\6	182.5	0.0	100.5	9.2	345, 8	182.3	2.4	
15	14.32	87.17	5\5\5	176.0	-10.5	73.1	9.0	300, 7	177.0	-4.6	
16	14.34	87.17	3\5\5	182.4	-15.3	71.3	14.7	300, 7	183.9	-9.1	
			8\10\10	178.4	-12.6	65.7	6.9		179.0	-6.6	
17	14.34	87.17	5\5\5	189.3	-18.8	127.8	6.8	300, 7	190.0	-12.9	
18	14.44	87	3\4\4	330.0	7.1	175.9	9.3	114, 10	328.6	12.9	
19	14.44	87	5\5\5	333.2	19.8	75.2	8.9	114, 10	329.8	25.9	
20 ^a	14.45	87	1	348.6	0.9			114, 10	348.1	9.0	
21	14.41	87.12	3\3\3	175.5	-15.0	42.2	19.2	136, 13	171.9	-23.0	
22	14.41	87.12	3\3\3	159.2	-11.1	74.5	14.4	136, 13	156.3	-15.9	
23 ^a	14.44	87.16	4\5\5	309.4	29.5	16.4	23.4	128, 24	296.3	27.3	
24 ^a	14.46	87.17	3\3\3	353.6	8.1	32.7	21.9	128, 24	348.4	24.6	
25	14.46	87.21	3\4\5	172.8	17.5	107.0	12.0	101, 7	173.3	10.8	
26	14.46	87.21	5\5\5	353.4	46	41.1	12.1	101, 7	350.8	52.6	
27	14.46	87.22	4\4\5	186.2	-16.5	48.5	13.3	110, 6	185.7	-22.3	
28	14.45	87.23	3\3\4	357.6	8.6	19.7	14.3	110, 6	357.1	14.1	
29 ^a	14.46	87	2\2\4	329.6	28.9			100, 23	316.8	44.9	
30 ^a	14.46	87	2\2\4	183.4	-16			100, 23	181.8	-38.8	
31 ^a	14.46	87	1	262.2	12.5			100, 23	258.9	4.7	
32	14.46	86.99	4\4\4	328.7	-4.7	108.4	8.9	102, 32	325.9	18.4	
33	14.46	86.99	4\5\5	327.1	-4.3	103.6	9.1	115, 28	325.8	10.5	
			8\9\9	327.9	-4.5	121.8	5.0		325.8	14.5	
34	14.47	86.98	5\6\5	178.8	9.9	43.3	11.8	94, 23	178.7	-13.0	
35	14.47	86.98	3\3\4	327.9	6.4	64.3	12.3	80, 29	323.5	32.9	
36	14.42	87.1	3\4\4	180.2	36.7	196.4	8.8	145, 8	184.5	31.8	
37	14.42	87.1	3\3\4	349.9	26.4	87.6	9.1	145, 8	346.0	29.5	
38	14.41	87.1	3\4\4	344.4	20.5	42.7	19.1	270, 4	344.8	16.6	
39	14.41	87.11	3\3\3	177.8	-9.5	181.2	9.2	sub hoz	177.8	-9.5	
40	14.41	87.11	4\5\5	187.8	-20.3	59.9	12.0	136, 13	183.8	-30.3	
41	14.41	87.12	5\5\5	183.5	-9.4	32.0	13.7	136, 13	181.2	-18.8	
Overall	14.39	87.14	36	350.1	13.2	11.2	7.5		349.4	18.4	10.3; 7.7
Selected			33	352.8	13	19.7	5.8		352.5	15	16.6; 5.8
Reference direction		356.6, 23.1		(ΔDx = 3.2; ΔIx = 5.6)		ΔDx = 4.8, ΔIx = 9.1		R = -4.1 +/- 6.1 F = -8.6 +/- 11.3		ΔDx = 5.2, ΔIx = 9.8	
Normal			16						342.5	19.8	20.4; 8.4
Reverse			17						181.3	-10.1	23.1; 7.6

^a Indicates sites excluded from final calculations.

and typical signals were at least two orders of magnitude higher. The back-field demagnetization curve was measured up 100 mT back field which is well beyond the remanent coercive force (B_{cr}) with an increment of 2 mT. For the hysteresis loops, the applied maximum field was 2 T and the field increment 2 mT, correction for pole shoe saturation was applied for data higher than 1.5 T on the basis of a linear slope between 1 and 1.5 T. After this correction the hysteresis loops were corrected for the paramagnetic slope by forcing the high-field slope to become horizontal using the data from 1.4 T upwards. From the slope-corrected loop the coercive force (B_c), the saturation magnetization (M_s) and remanent saturation magnetization (M_{rs}) were determined. This enables calculation of the M_{rs}/M_s and B_{cr}/B_c ratios that are indicative of magnetic grain size (Day et al., 1977). Further IRM acquisition curves were determined with the robotized 2G SQUID magnetometer system with in-line alternating field demagnetization equipment, and equipment for the acquisition anhysteretic remanent magnetization (ARM) and IRM, developed in the Utrecht paleomagnetic laboratory. The instrumental noise level is $\sim 3e^{-12} \text{ Am}^2$ and IRM signals

were at least 5 orders of magnitude higher. The IRM acquisition curves were fitted with the software developed by Kruiver et al. (2001) that allows fitting of cumulative log-Gaussian distributions to the measured data. It was experimentally shown by Robertson and France (1994) that IRM acquisition curves can reasonably well be approximated by cumulative log-Gaussian distributions. Each coercivity distribution is characterized by three parameters: the saturation IRM (SIRM or M_{rs}) indicating the amount of the component, the remanent acquisition coercive force ($B1/2$) indicating the mid-point of the coercivity distribution (or switching field distribution), which can be tied to the minerals involved, and the dispersion parameter (DP) indicating the width of the coercivity distribution that provides information on the crystallinity of the magnetic minerals involved. Deviations from the log-normal distributions are caused by thermal activation processes in very small magnetic particles and/or by magnetic interaction (Egli, 2004; Heslop et al., 2004). These deviations are minimized when the alternating field demagnetized starting state is adopted (Heslop et al., 2004). This was done here: prior to the IRM acquisition the samples were statically AF

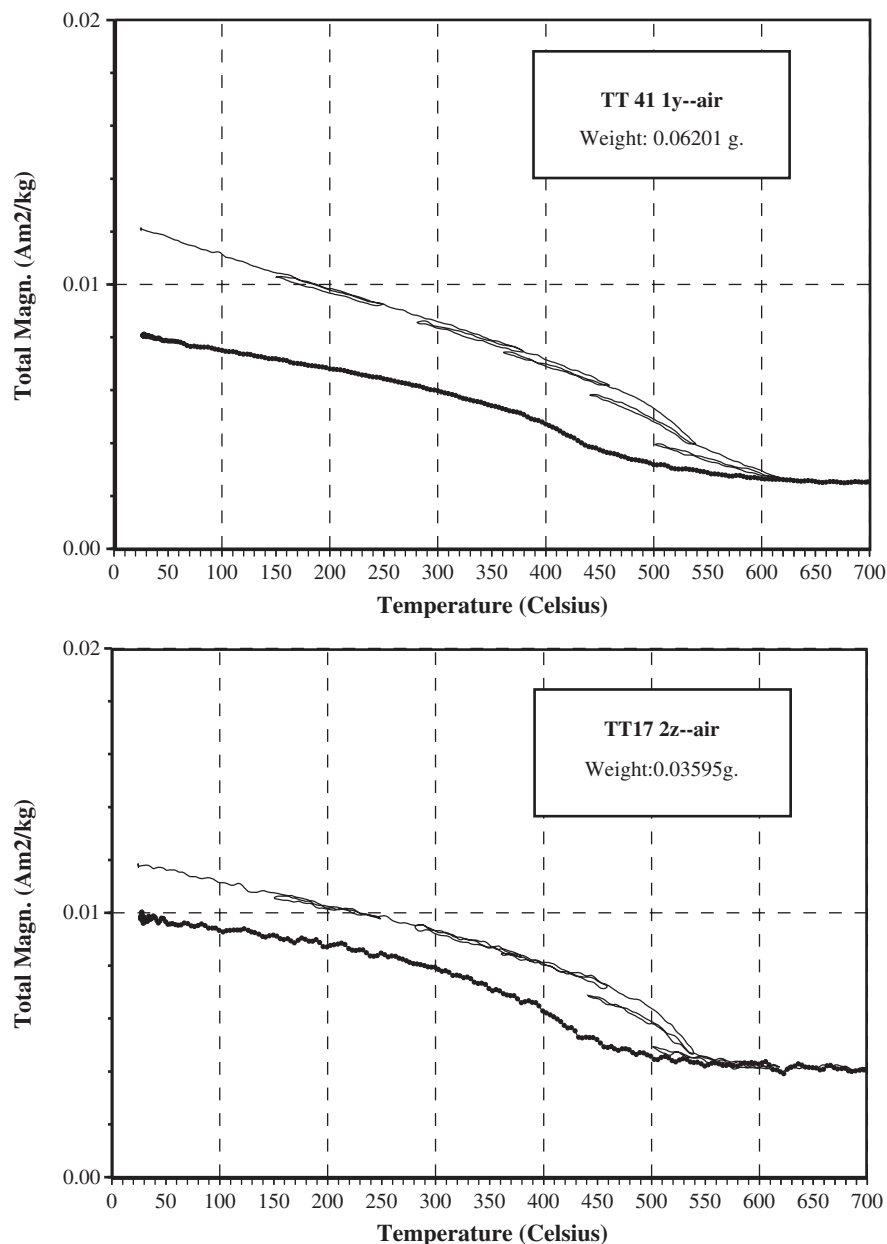


Fig. 5. Thermomagnetic curves of selected ignimbrite samples. The heating curve is the thin line.

demagnetized at 300 mT in three orthogonal directions with the last demagnetization axis parallel to the IRM acquisition direction. IRM acquisition was done in 61 steps up to 700 mT with the 2G long-core pulse magnetizer attached to the robotized magnetometer system. Because the rhyolites are not strongly magnetic, magnetic interaction is considered less important, and deviations from log-normality are primarily interpreted in terms of small magnetic particles.

The natural remanent magnetization (NRM) of one group of samples was measured with a 2G Enterprise cryogenic magnetometer at the Paleomagnetic Laboratory Fort Hoofddijk (University of Utrecht). These samples were subjected to stepwise alternating field (AF) demagnetization using the “on line” AF demagnetizing coils of the 2G Enterprise system. For a second set of samples we used a JR5 spinner magnetometer (AGICO, Brno, Czech Republic) for NRM measurements, and samples were subjected to stepwise thermal demagnetization using a non-inductive ASC TD-48-SC furnace. These measurements were conducted at the paleomagnetic laboratory of the Centro de Geociencias (Universidad Nacional Autónoma de México).

Orthogonal demagnetization diagrams (Zijderveld, 1967) were visually inspected to determine the vector composition of the remanent magnetization; principal component analysis (Kirschvink, 1980) was used to determine the direction of the characteristic magnetization (ChRM). Site means and the overall mean were determined using Fisher statistics (Fisher, 1953), and also using the method proposed by Deenen et al. (2011) who suggest instead the use of the distribution of virtual geomagnetic poles (VGPs).

5.2. Rock magnetism: results and interpretation

After correction for the contribution of the empty furnace and sample tube, the signal in the susceptibility versus temperature appeared to be very close to the limit of detection of the instrument, resulting in noisy curves that are difficult to interpret unambiguously. During the cycling up to 400 °C reversible behavior is measured, while thermal cycling up to 700 °C indicates some chemical alteration (curves not shown here). Thermomagnetic analyses yield well-interpretable results (typical signal-to-noise ratio at least two orders of magnitude above noise level). In two samples a ferromagnetic component of the signal could not be resolved reliably (material from TT9 and 25). In samples TT17.2z, TT36.2z and TT41.1y a meaningful ferromagnetic component is measured. These thermomagnetic curves are very similar in behavior (Fig. 5) and indicate no alteration up to 380 °C (completely reversible curves) while minute alteration to a less magnetic phase is measured after annealing to 460 °C. This alteration is more pronounced after heating to 540 °C and 620 °C. This makes it impossible to detect a formal Curie temperature; the oxidation creates a magnetization ‘tail’ to temperatures of >600 °C indicative of partially oxidized (magnetized) magnetite. The notable decay in magnetization only at temperatures over 500 °C points to a titanium-poor or titanium-free magnetite perfectly compatible with the rhyolitic rocks under study. After heating to 700 °C the cooling branch indicates a much lower magnetic ordering temperature than the heating segments possibly related to a disordered crystal structure.

The shape of the hysteresis loops is regular with a large paramagnetic contribution, no wasp-waisting is observed. Ms values range from $\sim 0.8 \cdot 10^{-3}$ to $\sim 15 \cdot 10^{-3}$ Am²/kg; visibly the slightly weathered material appears to have lowest mineral magnetic content. Bc and Bcr values are in good agreement with those expected for fine-grained ferrimagnetic oxides. Sites TT9 and TT25 seem to be affected by incipient weathering, they have the highest coercivities. All samples plot in the lower part of the pseudo-single-domain (PSD) region (Day et al., 1977) pointing at paleomagnetically stable NRM (Fig. 6).

IRM acquisition curves are close to saturation with inductions of 300 mT (Fig. 7), but in some of the samples there is a contribution from a high coercivity phase. IRM component fits (not shown) concur

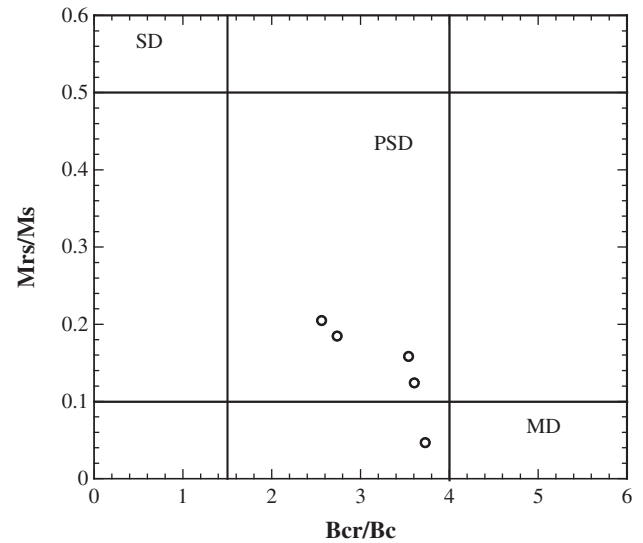


Fig. 6. Day plot (Day et al., 1977) of selected samples of the Padre Miguel Group ignimbrites.

with the hysteresis loop data; IRM acquisition curves are dominated by a low-coercivity component, referred to as component 1. Its contribution is at least 70% of the total IRM, but more typically it is 85 to 90%. It has B1/2 values ranging between 65 and 85 mT indicating fine-grained ferrimagnetic oxides (the incipiently weathered samples have lower B1/2 and slightly larger DP than the others). DP values of ~ 0.26 (log units) point to a grain-size distribution in line with crystallization from a magma (biogenic particles with a very narrow size distribution have a distinctly lower DP of <0.18). Component 2 that occurs in amounts up to $\sim 14\%$, has a lower coercivity than component 1 (B1/2 ~ 20 mT); it is considered an artifact of a skewed-to-the-left coercivity distribution due to thermal activation (Egli, 2004; Heslop et al., 2004) that has to be fitted with an extra IRM component in the software package utilized. So, component 2 has no physical meaning, the amount can be added to that of component 1. Component 3, the high coercivity component is rather variable in its properties, in part related to its low proportional occurrence. It is as much as 26% of the IRM in the sample from site TT25. B1/2 values of ~ 250 mT are

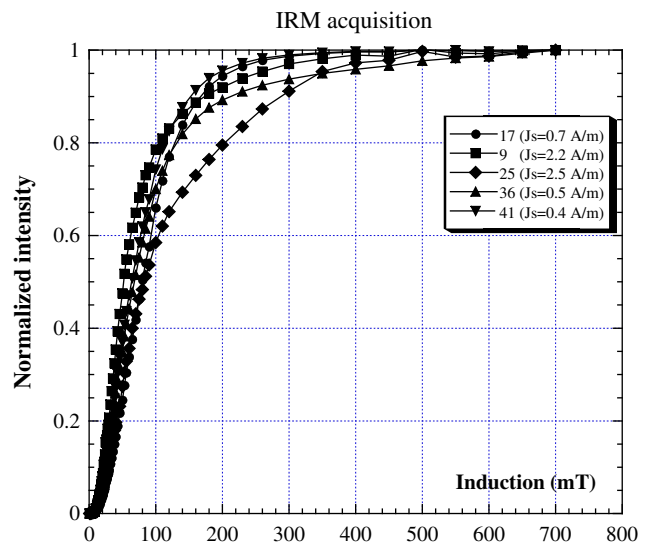


Fig. 7. IRM acquisition curves of selected samples of the Padre Miguel Group ignimbrites.

typical. This could be a small contribution of an antiferromagnetic mineral. This component may be considered to be associated with fluid movement through the rock that has resulted in a high-

coercivity partially maghemitized titanomagnetite, but also to deuteritic oxidation. The two sites showing incipient weathering have the highest proportional contribution of component 3.

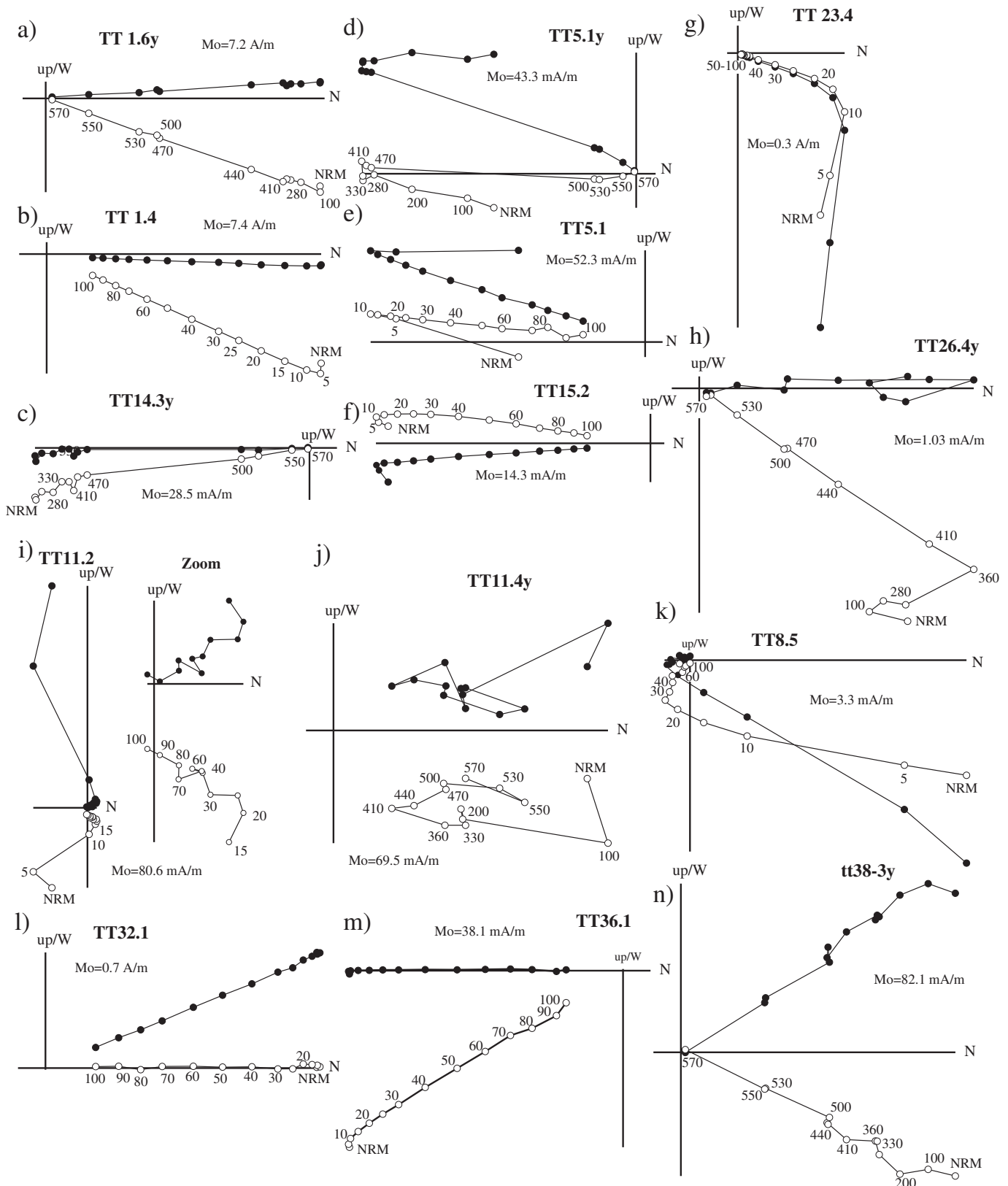


Fig. 8. Orthogonal demagnetization diagrams (Zijderveld, 1967) of selected ignimbrite samples of the Padre Miguel Group. Solid (open) symbols are projections of the horizontal (vertical) plane. Steps marked in °C or mT.

5.3. Demagnetization behavior

Samples from the Padre Miguel ignimbrites are characterized by NRM intensities ranging from a 0.7 mA/m in the weakly magnetized samples to 2.4 A/m in the strongly magnetized samples. Nearly all sites respond well to AF and thermal demagnetization. In about 90% of the sites, the magnetization is univectorial with well-defined linear trends to the origin (e.g., Fig. 8a, b and c). Samples with this behavior exhibit relatively high median destructive fields of 40 to 55 mT, and maximum coercivities of the NRM in excess of 100 mT (e.g., Fig. 8c, f and m). Thermal demagnetization of samples from the same sites show distributed unblocking temperatures between 400 and 570 °C (Fig. 8a, b and n). Maximum unblocking temperatures at nearly all sites are 570 °C; higher values were observed in sites TT11, TT25, TT27 and TT28. The magnetization that unblocked between 400 and 570 °C (or 25–100 mT) is considered the ChRM; it is north directed and has a moderately shallow positive inclination, or its antipode. Maximum angular deviation values in the PCA of the ChRM are typically less than 2°.

In a smaller percentage of sites there are low-stability secondary magnetizations considered overprints of recent origin, viscous or isothermal (lightning induced). Examples such as Fig. 8d and e show that these secondary magnetizations are easily removed with inductions of 10 to 20 mT or heating to 300 °C. But occasionally, these magnetizations are of high intensity, preventing complete isolation of the ChRM (e.g., Fig. 8i and k; for sites TT11 and TT8, respectively). In cases such as sites TT8 and TT5 the overprint is north directed and appears to be of viscous origin. Demagnetization trajectories define great circles and these converge to define a ChRM. In cases such as site TT23 (Fig. 8g) the overprint is east directed and steep, more likely induced by lightning. The behavior observed in site TT11 is relatively complex. Most samples show multivectorial magnetization with low coercivity randomly oriented magnetization, an intermediate coercivity north-west directed magnetization (Fig. 8i), and a magnetization not resolved by AF demagnetization – which appears to lie in the SE quadrant. Thermal demagnetization experiments confirm that the magnetization not resolved by AF on site TT11 is south directed and shallow, but the ChRM in this site is considered the intermediate coercivity north directed magnetization; the high coercivity component is considered an overprint, perhaps related to weathering.

Sample directions are relatively well grouped at the site level. While at all 41 sites we obtained a mean direction, after final comparison of the site means, visual inspection of hand samples, and their

demagnetization behavior it was determined that the pair of sites TT12–TT13 represent statistically indistinguishable results and probably represent the same cooling unit; these site pairs were combined (Fig. 9; Table 1). This yields a total of 40 spot readings of the Middle Miocene geomagnetic field. The site means of 4 sites are represented by only one or two samples, the rest were lost during transport, and three more yield poor statistics ($k < 30$ and $\alpha_{95} > 20^\circ$) and were excluded from the final calculations. This leaves a total of 33 sites, 16 of normal polarity and 17 of reverse polarity. Although no attempt was made to build a magnetic polarity zonation, sites 1 through 17 appear to define a continuous stratigraphic section that includes two magnetozones of normal polarity and two of reverse polarity.

The distribution of virtual geomagnetic poles (VGPs) fits well a Fisher distribution providing an overall mean direction (tilt corrected) of $D \pm \Delta D_x = 352.5 \pm 5.2^\circ$ and $I \pm \Delta I_x = 15.0 \pm 9.8^\circ$ ($n = 33$, $K_{vgp} = 24.5$, and $A_{95(vgp)} = 5.2^\circ$ Table 1, see Deenen et al., 2011 for an explanation of this nomenclature). If we compare this result to the n -dependent reliability envelope of Deenen et al. (2011), we conclude that scatter of our data can be straightforwardly explained by paleosecular variation (PSV): $A_{95, \text{observed}} = 5.2^\circ$, which falls between the $A_{95\text{min}}$ (4.2°) and $A_{95\text{max}}$ (9.1°) values for $n = 33$. In other words, there is no statistical need to infer sources of scatter besides PSV (such as internal rotations) to explain our data set. We note, however, that comparing the normal and reversed directions yields a negative reversal test. Shallower inclinations in the reverse polarity magnetization suggest that incomplete removal of a normal polarity overprint could explain a negative test, but the bulk of the difference is in declination and this is further discussed below. If a similar overprint acts on the normal and reverse polarity sets, its effect is likely canceled. The elongation observed in the distribution of sample directions ($E = 1.584$) is lower than expected for this latitude ($\sim 14^\circ$) according to paleosecular variation (PSV) models that consider a systematic variation of dispersion with latitude (e.g., Tauxe and Kent, 2004). Elongation–inclination analysis suggest that the f factor that makes adequate the distribution to the expected field model is $0.55^{+-.17/-0.14}$. However, this analysis is typically applied to sedimentary rocks, not to igneous rocks and requires much larger ($n > 100$) data sets than we obtained. The angular standard deviation of the VGP distribution ($\sim 16.5^\circ$) suggests that sampling of PSV is sufficient (for the paleolatitude of the sampling area). Nonetheless, a lower value for reverse polarity magnetizations (13°), as well as an A_{95} value (5.3°) slightly below $A_{95\text{min}}$ (5.5° at $n = 17$) in turn suggests that the reversed population does not sufficiently average PSV (Deenen et al., 2011).

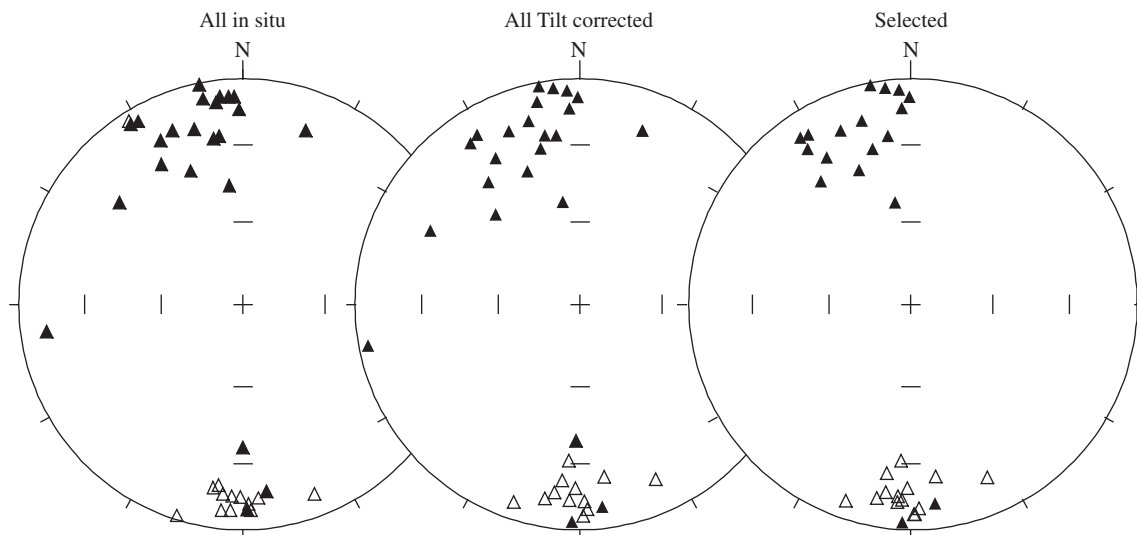


Fig. 9. Stereographic projections of site mean in situ and tilt corrected. Solid (open) symbols are projections on the lower (upper) hemisphere. Selected sites correspond to sites with $k > 30$ and $\alpha_{95} < 20^\circ$ (tilt corrected).

Table 3
Miocene paleomagnetic data for the Caribbean region.

Rock unit	N/n	Age	P lat	P long	A95	R	ΔR	F	ΔF	Reference
Padre Miguel Group, Honduras	33 s/129	14–17 Ma	80.0	142.9	5.2					1
North America reference			85.9	146.8	3.2					2
Las Yayas Andesite, Dominican Republic	4 s/44	5–23 Ma	78.5	230.6	11.5	−5.1	13.8	22.6	15.9	3
Coyol Group, Nicaragua	7 s/47	~18 Ma	78.9	93.5	8.4	7.7	13.0	8.6	7.9	4
Low Laton Lavas, Jamaica	5 s/95	5–15 Ma	73.3	208.6	7.4	−12.0	9.7	16.6	10.9	5
Caribbean plate mean	4	~15 Ma	82.3	179.4	K = 49.6, A95 = 13.2					

1 This study; 2 Besse and Courtillot (2002); 3 Vincenz and Dasgupta (1978); 4 Elming et al. (2001); 5 Guja and Vincenz (1978).

Comparing the mean directions for the three geographic areas may suggest internal vertical axis rotations within our study area, but the data sets for individual areas are not sufficiently robust. The western and central areas, with 13 and 11 sites respectively, yield statistically north-directed indistinguishable means. The eastern area with only five sites yields a distinct northwest-directed mean, but this may reflect insufficient average of PSV at this level. We therefore explain the negative reversal test by insufficient averaging of paleosecular variation in the normal and reversed data sets alone and because the combined data set yields statistical values that are perfectly in line with PSV, we consider our combined pole reliable, at lat = 80.0°N, lon = 142.9°E, K = 24.5, A₉₅ = 5.2°.

6. Discussion

To determine relative motion between the studied area in the Chortis Block and the North American plate, we compared the Miocene grand mean direction we obtained from the Padre Miguel Group with the expected direction at 15 Ma (interpolated between 10 and 20 Ma using the global apparent polar wander path of Torsvik et al (2008)) for the North American plate at a central reference location

in the study area (14.39°N, 87.14°W). The integrated mean pole for North America at 15 Ma is 85.92°N/146.8°E, A₉₅ = 3.16°, yielding an expected North American direction for the reference site of $D \pm \Delta D_x = 356.6 \pm 3.2^\circ$, $1 \pm \Delta l_x = 23.1 \pm 5.6^\circ$. We calculated rotation (R) and flattening (F) estimates, obtaining $R \pm \Delta R = 4.1^\circ \pm 6.1^\circ$ and an $F \pm \Delta F = -8.1^\circ \pm 11.3^\circ$. These indicate insignificant rotations and paleolatitudinal motions since middle Miocene time. This shows that the nearly west to east motion of Chortis relative to North America along the Polochic–Motagua–Cayman fault zone did not lead to significant vertical axis rotations of the central Honduras highlands (and by extrapolation the stable portion of the Chortis Block) since Middle Miocene time.

The Caribbean plate lacks high quality paleomagnetic data for the Neogene. Available studies commonly include a small number of sites in uncertain tectonic setting (Elming et al., 2001; Guja and Vincenz, 1978; Vincenz and Dasgupta, 1978; Table 3 and Fig. 10). A critical view of the data sets from Jamaica, Dominican Republic, and the Nicaragua highlands, suggests that these data pass minimum reliability criteria (Q = 3; Van der Voo, 1990). But the data from Jamaica and Dominican Republic (LL and LY) include only reverse polarity magnetizations, and all three locations studied lack good structural control,

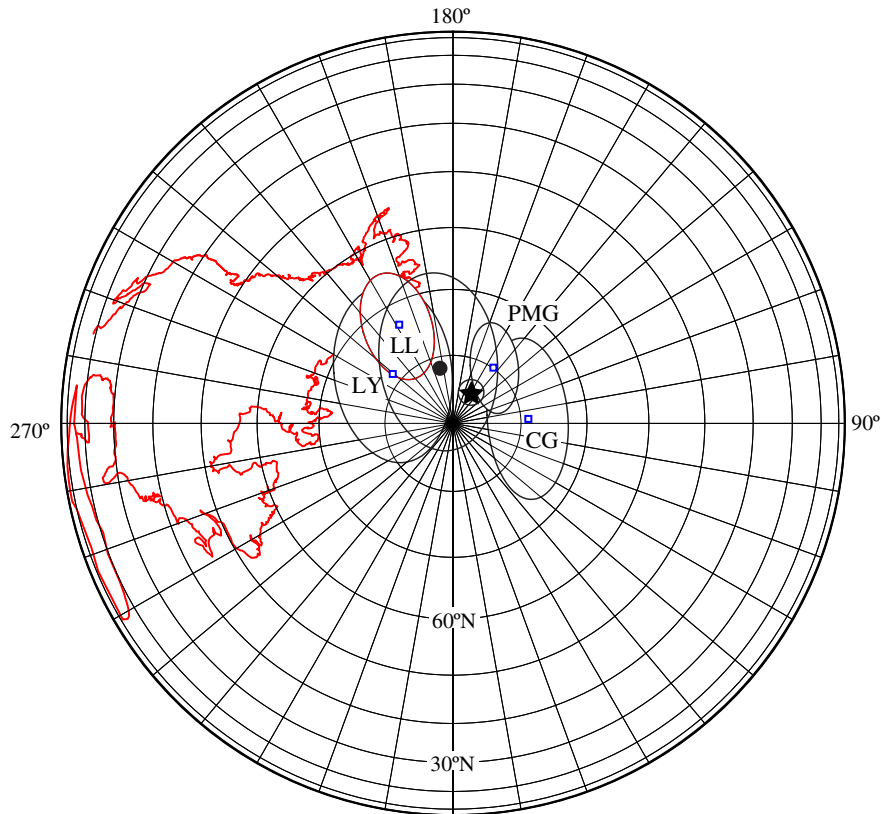


Fig. 10. Miocene paleomagnetic poles for the Caribbean plate compared to the (~15 Ma) North America reference (star) poles. Symbols are: LY = Las Yayas Andesite (Vincenz and Dasgupta, 1978); LL = Low Laton Lavas (Guja and Vincenz, 1978); CG = Coyol Group (Elming et al., 2001); PMG = Padre Miguel Group. Poles include their 95% confidence interval. The average of these four poles is shown as a solid circle. All poles are listed in Table 3.

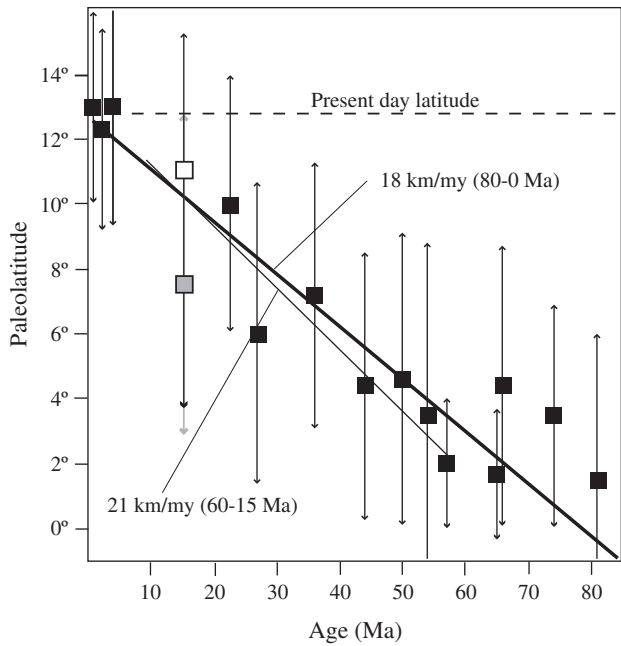


Fig. 11. Estimate of northward motion of the Caribbean plate, calculated for ODP site 999. Data for Padre Miguel Group gray square. Paleolatitude calculated for a mid-Miocene paleopole is a white square. Modified from Acton et al. (2000).

particularly sites in the Nicaragua Highlands. The poles LL and LY are near-sided, while the Nicaragua pole is far-sided. The average of these three poles (82.1°N–194.3°E) is indistinguishable from the Padre Miguel grand mean (80.0°–142.9°E), but carries a large A_{95} of ~20°.

Our first approach to the Caribbean paleomagnetic data set for the mid-Miocene was to estimate rotation and flattening parameters for the Jamaica, Dominican Republic, and Nicaragua highlands with respect to central Chortis (Table 3). The results do not provide consistent information. Large latitudinal displacements are suggested by F values, both northward and southward. Such displacements are not warranted by plate tectonic models (e.g. Pindell and Kennan, 2009). Most likely, paleosecular variation may not be sufficiently averaged in those studies. Our conclusion is that additional paleomagnetic data from the Antilles islands is required to evaluate intra-plate deformation, or determine if

deformation in the islands involves significant rotations about vertical axes.

As a second approximation, we combined all four poles, so we can define a Middle Miocene pole (~15 Ma) for the Caribbean plate; the pole is located at 82.3°N–179.4°E ($K=49.6$ and $A_{95}=13.2^\circ$). The pole predicts, for instance, a paleolatitude of $11.1^\circ \pm 6.6^\circ$ for ODP Site 999 (12.74°N/281.26°E), which has been studied paleomagnetically by Acton et al. (2000). This paleolatitude suggests that the net rate of poleward motion of the Caribbean plate since the Middle Miocene is negligible (less than 1°); although including the Miocene data in the regression line adjusted by Acton et al. (2000) for the northward drift of the Caribbean since about 80 Ma to present is well within their estimated rate of about 18 km/my, data for Miocene volcanic rocks around the Caribbean suggest a faster rate of northward motion for the Paleocene–Early Miocene interval (21 km/my, Fig. 11), and very small northward motion since the Middle Miocene. Because Miocene northward displacement of a point on the southern edge of the North America plate is small (on the order of 200 km), a similar small displacement on the Caribbean plate during the Miocene does not require significant compression along the Cayman trough. Although our Miocene data improves the estimates of Miocene to recent poleward motion of the Caribbean, for earlier times more data are required. Overall, the constant northward drift for Paleocene–Oligocene time of Fig. 11, which is based on Acton et al. (2000), cannot be confirmed by quality paleomagnetic data for Cretaceous–Oligocene time from elsewhere in the Caribbean plate and may be questioned on tectonic grounds.

Burkart (1983) suggested that the Polochic fault system accommodated ~130 km of sinistral displacement in the Neogene. They suggested that displacement is supported by the correlation of geologic features on both sides of the fault, most notably the Paleozoic cored Chicomuselo uplift in Chiapas and the Tactic-Santa Rosa anticlinorium in Guatemala, and the Miocene volcanic arcs of southern Mexico and Central America. The Cayman Trough (CT) accommodated the motion between the Caribbean and North America between 49 Ma and the present (Leroy et al., 2000; Rosencrantz et al., 1988).

The rate of spreading in the CT has been estimated at ~20 mm/yr in the last 2 Ma, but the older opening rates are controversial. Leroy et al. (2000) modeled marine magnetic anomalies in the CT using a half-spreading rate of 8.5 mm/yr from the present to about 20 Ma. We thus restored the Chortis Block 255 km along the Polochic–Motagua system, to its position 15 Ma. This places the northwest

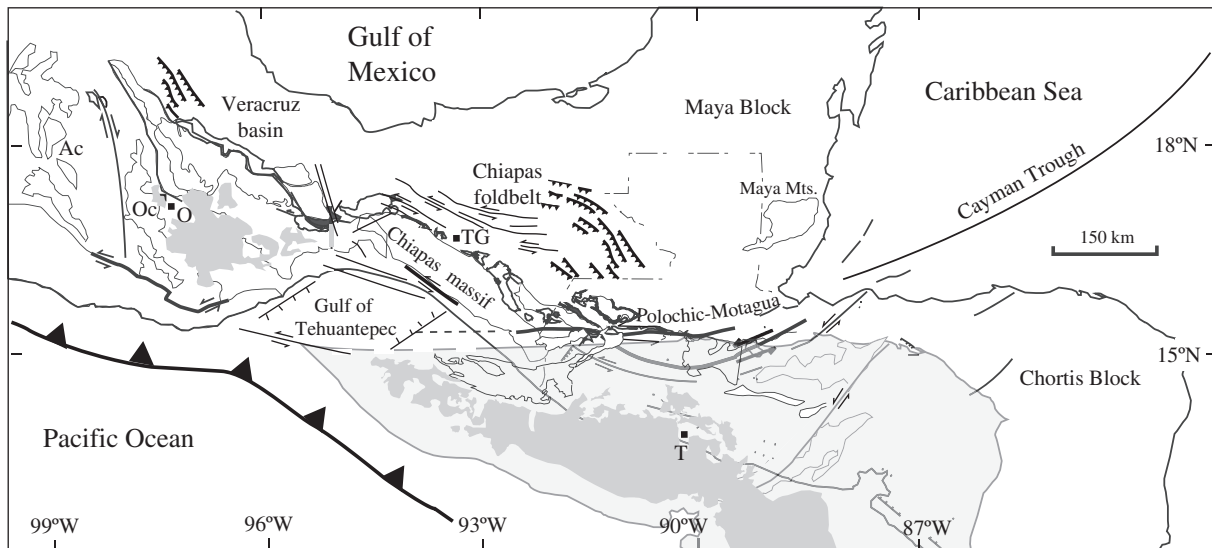


Fig. 12. Reconstruction of the Chortis Block relative to southern Mexico 15 Ma. Dark gray pattern shows the distribution of mid-Miocene rhyolitic volcanism. Also the present-day coastal outlines, structural features, and some basement elements are provided (O = Oaxaca; T = Tegucigalpa; TG = Tuxtla Gutiérrez; Oc Oaxaca Complex; Ac = Acatlan Complex).

end of the Chortis Block in the area of the Gulf of Tehuantepec (Fig. 12). The reconstruction aligns, as Burkart (1983) had already noted, the Central America ignimbrite province with the Miocene ignimbrite province of east-central Oaxaca, for which published ages range between about 13 and 20 Ma (Morán-Zenteno et al., 2000), i.e. similar to our findings (Fig. 4, Table 1). In this reconstruction there is no overlap between the northern termination and the Tehuantepec basin. The Tehuantepec basin is a NW–SE depocenter between the southeast moving Chortis Block and the Chiapas Massif, and it probably opened as a pull-apart basin controlled by the Tonalá shear zone on the north (Wawrzyniec et al., 2005) and the Polochic system on the south. The Tehuantepec basin contains a thick record of coarse-grained Miocene continental sedimentation, and it is bounded by a major normal fault on the north and first order strike-slip faults on the east and west (Sánchez-Barreda, 1981; Silva-Romo and Mendoza-Rosales, 2009). Our paleomagnetic and geochronological studies hence support models proposing that ~250 km of post-middle Miocene displacement of the Chortis Block relative to north America explains the offset of the Miocene ignimbrite belt of central America. This motion was not associated with wholesale rotation or paleolatitudinal displacement of Chortis.

7. Conclusions

We present new $^{40}\text{Ar}/^{39}\text{Ar}$ age constraints from the Padre Miguel ignimbrites covering the Chortis Block of central Honduras of 16.1 ± 0.2 Ma and 14.42 ± 0.08 Ma. These ignimbrites carry dual polarity magnetizations. Rock magnetic data are consistent with a thermoremanent magnetization residing primarily in a cubic phase such as Ti-poor magnetite. The complete set of 33 spot observations (reference location 14.39°N , 87.14°W) of the Middle Miocene field direction defines a paleomagnetic pole at $80.0^\circ\text{N}/142.9^\circ\text{E}$ ($K = 24.5$, $A_{95} = 5.2$). The observed mean direction is not statistically distinguishable from the expected direction of the North America craton, R and F parameters $R = -4.1^\circ \pm 6.1^\circ$ and an $F = -8.6^\circ \pm 11.3^\circ$ indicate insignificant rotation or latitudinal displacement. We present new $^{40}\text{Ar}/^{39}\text{Ar}$ ages showing that the Padre Miguel ignimbrites in the sampling area were emplaced between about 14 and 17 Ma. Restoring ~250 km of eastward motion of the Chortis Block following Cayman trough reconstructions brings the Padre Miguel ignimbrites into alignment with the Miocene volcanic arc rocks of southern Mexico (Oaxaca). We conclude that the offset of the Middle American volcanic arc resulted from Caribbean–North American plate motions, and that these motions did not lead to local or regional vertical axis rotations.

Acknowledgments

This research was partially supported by a PAPIIT-UNAM grant IN106807 to RSMG. DJJvH acknowledges Statoil for their financial support (SPlates Model project). We thank the journal editor Mian Liu, Ruben Somoza and an anonymous reviewer for the comments to the manuscript.

Appendix A. Supplementary data

Supplementary data to this article can be found online at <http://dx.doi.org/10.1016/j.tecto.2012.08.013>.

References

Acton, G.D., Galbrun, B., King, J.W., 2000. Paleolatitude of the Caribbean plate since the Late Cretaceous. In: Leckie, R.M., Sigurdsson, H., Acton, G.D., Draper, G. (Eds.), *Proceedings of the Ocean Drilling Program: Scientific Results*, 165, pp. 149–173.

- Besse, J., Courtillot, V., 2002. Apparent and true polar wander and the geometry of the geomagnetic field over the last 200 Myr. *Journal of Geophysical Research* 107, 2300 <http://dx.doi.org/10.1029/2000JB000050>.
- Burkart, B., Clemons, R.E., 1973. Mesozoic and Cenozoic stratigraphy of Southeastern Guatemala. *AAPG Bulletin* 57 <http://dx.doi.org/10.1306/819A4248-16C5-11D7-8645000102C1865D>.
- Burkart, B., 1983. Neogene north American–Caribbean plate boundary across Northern Central America: offset along the polochic fault. *Tectonophysics* 99, 251–270.
- Burkart, B., Self, S., 1985. Extension and rotation of crustal blocks in northern Central America and effect on the volcanic arc. *Geology* 13, 22–26.
- Cande, S.C., Kent, D.V., 1995. A revised calibration of the geomagnetic polarity timescale for the Late Cretaceous and Cenozoic. *Journal of Geophysical Research* 100, 6093–6095.
- Case, J.E., Holcombe, T.L., 1980. *Geologic–Tectonic Map of the Caribbean Region*, Reston, Va. United States Geological Survey.
- Day, R., Fuller, M., Schmidt, V.A., 1977. Hysteresis properties of titanomagnetites: grain-size and compositional dependence. *Physics of the Earth and Planetary Interiors* 13, 260–267.
- Deenen, M.H.L., Langereis, C.G., van Hinsbergen, D.J.J., Biggin, A.J., 2011. Geomagnetic secular variation and the statistics of palaeomagnetic directions. *Geophysical Journal International* 186, 509–520.
- DeMets, C., Mattioli, G., Jansma, P., Rogers, R.D., Tenorio, C., Turner, H.L., 2007. Present motion and deformation of the Caribbean plate: constraints from new GPS geodetic measurements from Honduras and Nicaragua. *Geological Society of America Special Paper* 428, 21–36.
- Dengo, G., 1969. Problems of tectonic relations between Central America and the Caribbean. *GCAGS Transactions* 19 <http://dx.doi.org/10.1306/A1ADF38F-ODFE-11D7-8641000102C1865D>.
- Egli, R., 2004. Characterization of individual rock magnetic components by analysis of remanence curves. 2. Fundamental properties of coercivity distributions. *Physics and Chemistry of the Earth* 29, 851–867.
- Ehrenborg, J., 1986. A new stratigraphy for the Tertiary volcanic rocks of the Nicaraguan Highland. *Geological Society of America Bulletin* 108, 830–842.
- Elming, S.A., Layer, P., Ubieta, K., 2001. A palaeomagnetic study and age determinations of Tertiary rocks in Nicaragua, Central America. *Geophysical Journal International* 147, 294–309.
- Emmet, P.A., 1983. *Geology of the Algateca quadrangle, Honduras, Central America*, unpubl. MA thesis, University of Texas, Austin, TX, USA, pp. 201.
- Engelbreton, D.C., Cox, A., Gordon, R.G., 1985. Relative motions between oceanic and continental plates in the Pacific Basin. *Geological Society of America Special Paper* 206, 59.
- Fisher, R.A., 1953. Dispersion on a sphere. *Proceedings of the Royal Society of London Series A* 217, 295–305.
- Guja, N.H., Vincenz, S.A., 1978. Paleomagnetism of some Late Cretaceous and Miocene igneous rocks on Jamaica. *Geophysical Journal of the Royal Astronomical Society* 52, 97–115.
- Guzmán-Speziale, M., Meneses-Rocha, J.J., 2000. The North America–Caribbean plate boundary west of the Motagua–Polochic fault system: a fault jog in Southeastern Mexico. *Journal of South American Earth Sciences* 13, 459–468.
- Heiken, G., Ramos, N., Duffield, W., Musgrave, J., Wohletz, K., Priest, S., Aldrich, J., Flores, W., Ritchied, A., Goff, F., Eppler, D., Escobar, C., 1991. *Geology of the platanares geothermal area, Departamento de Copán, Honduras*. *Journal of Volcanology and Geothermal Research* 45, 41–58.
- Herrmann, U.R., Nelson, B.K., Ratschbacher, L., 1994. The origin of a terrane: U Pb zircon geochronology and tectonic evolution of the Xolapa Complex (southern Mexico). *Tectonics* 13, 455–474.
- Heslop, D., McIntosh, G., Dekkers, M.J., 2004. Using time- and temperature-dependent Preisach models to investigate the limitations of modelling isothermal remanent magnetization acquisition curves with cumulative log Gaussian functions. *Geophysical Journal International* 157, 55–63.
- Jordan, B.R., Sigurdsson, H., Carey, S., Lundin, S., Rogers, R.D., Singer, B., Barquero-Molina, M., 2007. Petrogenesis of Central American Tertiary ignimbrites and associated Caribbean Sea tephra. *Geological Society of America Special Papers* 428, 151–179.
- Karig-Cordwell, D.E., Moore, G.F., Moore, D.G., 1978. Late Cenozoic subduction and continental margin truncation along the Middle America Trench. *Geological Society of America Bulletin* 89, 251–272.
- Keppie, J.D., Moran-Zenteno, D.J., 2005. Tectonic implications of alternative Cenozoic reconstructions for Southern Mexico and the Chortis Block. *International Geology Review* 47, 473–491.
- Kirschvink, J.L., 1980. The least-squares line and plane and the analysis of paleomagnetic data: examples from Siberia and Morocco. *Geophysical Journal of the Royal Astronomical Society* 62, 699–718.
- Kruiver, P.P., Dekkers, M.J., Heslop, D., 2001. Quantification of magnetic coercivity components by the analysis of acquisition curves of isothermal remanent magnetisation. *Earth and Planetary Science Letters* 189, 269–276.
- Lee, J.Y., Marti, K., Severinghaus, J.P., Kawamura, K., Yoo, H.S., Lee, J.B., Kim, J.S., 2006. A redetermination of the isotopic abundances of atmospheric Ar. *Geochimica et Cosmochimica Acta* 70, 4507–4512.
- Leroy, S., Mauffret, A., Patriat, P., Mercier de Lépinay, B., 2000. An alternative interpretation of the Cayman trough evolution from a reidentification of magnetic anomalies. *Geophysical Journal International* 141, 539–557.
- Malfait, B.T., Dinkelman, M.G., 1972. Circum-Caribbean tectonic and igneous activity and the evolution of the Caribbean plate. *Geological Society of America Bulletin* 83, 251–272.
- Mammerickx, J., Klitgord, D.K., 1982. Northern East Pacific rise: evolution from 25 my B.P. to the present. *Journal of Geophysical Research* 87, 6751–6759.

- Manton, W., 1996. The Grenville of Honduras. Geological Society of America Abstracts with Programs 28, A-493.
- McDougall, I., Harrison, T.M., 1999. Geochronology and Thermochronology by the $^{40}\text{Ar}/^{39}\text{Ar}$ method. Oxford University Press, New York.
- Meschede, M., Frisch, W., 1998. A plate-tectonic model for the Mesozoic and Early Cenozoic history of the Caribbean plate. Tectonophysics 296, 269–291.
- Morán-Zenteno, D.J., Martiny, B., Tolson, G., Solís-Pichardo, G., Alba-Aldave, L., Hernández-Bernal, M.S., Marcías-Romo, C., Martínez-Serrano, R.G., Schaaf, P., 2000. Geocronología y características geoquímicas de las rocas magmáticas terciarias de la Sierra Madre del Sur. Boletín de la Sociedad Geológica Mexicana. 53, 27–58.
- Mullender, T.A.T., Van Velzen, A.J., Dekkers, M.J., 1993. Continuous drift correction and separate identification of ferromagnetic and paramagnetic contributions in thermomagnetic runs. Geophysical Journal International 114, 663–672.
- Ortega-Gutiérrez, F., Solari, L.A., Ortega-Obregón, C., Elías-Herrera, M., Martens, U., Morán-Icálc, S., Chiquinc, M., Keppie, J.D., Torres De León, R., Schaaf, P., 2007. The Maya–Chortís boundary: a tectonostratigraphic approach. International Geology Review 49, 996–1024.
- Pindell, J.L., Barrett, S.F., 1990. Geological Evolution of the Caribbean Region; A Plate-Tectonic Perspective. Geological Society of America, The Geology of North America, Boulder, pp. 405–432. H.
- Pindell, J., Kennan, L., 2009. Tectonic evolution of the Gulf of Mexico, Caribbean and northern South America in the mantle reference frame: an update. In: James, K., Lorente, M.A., Pindell, J. (Eds.), The Geology and Evolution of the Region between North and South America: Geological Society of London, Special Publication, 328, pp. 1–57.
- Pindell, J.L., Cande, S.C., Pitman III, W.C., Rowley, D.B., Dewey, J.F., LaBrecque, J.L., Haxby, W.F., 1988. A plate-kinematic framework for models of Caribbean evolution. In: Scotese, C.R., Sager, W.W. (Eds.), Mesozoic and Cenozoic Plate Reconstructions: Tectonophysics, 155, pp. 121–138.
- Pindell, J.L., Maresch, W.V., Martens, U., Stanek, K.P., 2011. The Greater Antillean Arc: Early Cretaceous origin and proposed relationship to Central American subduction mélanges: implications for models of Caribbean evolution. International Geology Review 54, 131–143.
- Plafker, G., 1976. Tectonic aspects of the Guatemala earthquake of 4 February 1976. Science 24 (193), 1201–1208.
- Ratschbacher, L., Franz, L., Min, M., Bachmann, R., Martens, U., Stanek, K., Stübner, K., Nelson, B.K., Herrmann, U., Weber, B., López-Martínez, M., Jonckheere, R., Sperner, B., Tichomirowa, M., McWilliams, M.O., Gordon, M., Meschede, M., Bock, P., 2009. The North American–Caribbean plate boundary in Mexico–Guatemala–Honduras. Geological Society, London, Special Publication 328, 219–293.
- Renne, P.R., Mundil, R., Balco, G., Min, K.W., Ludwig, K.R., 2010. Joint determination of K-40 decay constants and Ar-40*/K-40 for the Fish Canyon sanidine standard, and improved accuracy for Ar-40/Ar-39 geochronology. Geochimica et Cosmochimica Acta 74, 5349–5367.
- Robertson, D.J., France, D.E., 1994. Discrimination of remanence-carrying minerals in mixtures, using isothermal remanent magnetisation acquisition curves. Physics of the Earth and Planetary Interiors 82, 223–234.
- Rodriguez, M., DeMets, C., Rogers, R., Tenorio, C., Hernandez, D., 2009. A GPS and modelling study of deformation in northern Central America. Geophysical Journal International 178, 1733–1754.
- Rogers, R., 2003. Jurassic–recent tectonic and stratigraphic history of the Chortis Block of Honduras and Nicaragua (northern Central America), unpubl. Ph.D. dissertation, University of Texas, Austin, 94 p.
- Rogers, R.D., Kárason, H., van der Hilst, R.D., 2002. Epeirogenic uplift above a detached slab in northern Central America. Geology 30, 1031–1034.
- Rogers, R.D., Mann, P., Emmet, P.A., 2007. Tectonic terranes of the Chortis Block based on integration of regional aeromagnetic and geologic data Boulder Geological Society of America, Special Paper 428, 65–88.
- Rosencrantz, E., Ross, M.I., Sclater, J.G., 1988. The age and spreading history of the Cayman trough as determined from depth, heat flow, and magnetic anomalies. Journal of Geophysical Research 93, 2141–2157.
- Sánchez-Barreda, L. A., 1981. Geologic evolution of the continental margin of the Gulf of Tehuantepec on southern Mexico: Ph.D. Thesis, University of Texas, Austin, Texas, pp. 192.
- Schaaf, P., Morán-Zenteno, D., Hernández-Bernal, M.S., 1995. Paleogene continental margin truncation in southwestern Mexico: geochronological evidence. Tectonics 14, 1229–1350.
- Silva-Romo, G., 2008. Guayape–Papalutla fault system: a continuous Cretaceous structure from southern Mexico to the Chortís Block? Tectonic implications. Geology 36, 75–78.
- Silva-Romo, G., Mendoza-Rosales, C., 2009. Evaluación geológica de los modelos para el truncamiento Cenozoico del sur de México: erosión por subducción y detachment del bloque Chortis. Revista Mexicana de Ciencias Geológicas 26, 165–176.
- Tauxe, L., Kent, D.V., 2004. A simplified statistical model for the geomagnetic field and the detection of shallow bias in paleomagnetic inclinations: was the ancient magnetic field dipolar. Geophysical Monograph 145, 1–15.
- Torsvik, T.H., Müller, R.D., Van der Voo, R., Steinberger, B., Gaina, C., 2008. Global plate motion frames: toward a unified model. Reviews of Geophysics 41, RG3004 <http://dx.doi.org/10.1029/2007RG000227>.
- Van der Voo, R., 1990. Reliability of paleomagnetic data. Tectonophysics 184, 1–9.
- Vincenz, S.A., Dasgupta, S.N., 1978. Paleomagnetic study of some Cretaceous and tertiary rocks on Hispaniola. Pure and Applied Geophysics 116, 1200–1210.
- Wadge, G., Burke, K., 1983. Neogene Caribbean plate rotation and associated Central American tectonic evolution. Tectonics 2, 633–643.
- Wawrzyniec, T., Molina-Garza, R.S., Geissman, J.W., Iriondo, A., 2005. A newly discovered relic, transform plate boundary – the Tonalá shear zone and paleomagnetic evolution of the western Maya Block, SW Mexico. Geological Society of America Abstract with Programs 37, 68.
- Williams, H., McBirney, A.R., 1969. Volcanic History of Honduras: Univ. Calif., Berkeley, Publ. Geol. Sci., 85, pp. 1–101.
- Williams, H., McBirney, A.R., Dengo, G., 1964. Geologic Reconnaissance of Southeastern Guatemala: Univ. Calif. Berkeley, Publ. Geol. Sci., 50, 62 pp.
- Zijderveld, J.D.A., 1967. A.C. demagnetization of rocks: analysis of results. In: Collinson, D.W., Creer, K.M., Runcorn, S.K. (Eds.), Methods in Rock Magnetism and Paleomagnetism. Elsevier, Amsterdam, pp. 254–286.